XENON REU at Nevis Labs, Columbia University

Juliette Alimena
Columbia University REU Program

I. INTRODUCTION

It is believed that baryons, which form ordinary, luminous matter, only represent about 4% of the composition of the universe; the rest is comprised of about 73% dark energy and 23% dark matter, both of which currently have unknown sources. Dark energy explains the acceleration of the expansion of the universe, while dark matter accounts for some "missing mass," whose presence can be inferred from gravitational effects on visible matter.

Zwicky is usually credited with proposing the modern idea of dark matter as a result of his studies of the Coma galaxy cluster in 1933 (see Figure 1). He discovered that many more times the luminous mass of the cluster is needed to keep the galaxies together. Another convincing source of evidence for dark matter is from the flat rotation curves of spiral galaxies (see Figure 2). In the late 1960s, Vera Rubin noticed that the rotational velocity of some spiral galaxies remains constant at large radii, despite the fact that the expected rotational velocity of a galactic disk falls off at large radii. However, the observed rotation curve can be explained if one sums the effects from gas, the galaxy disk, and a dark galactic halo. Other support for the concept of dark matter comes from the CMB anisotropies, supernova data, and weak gravitational lensing [1].

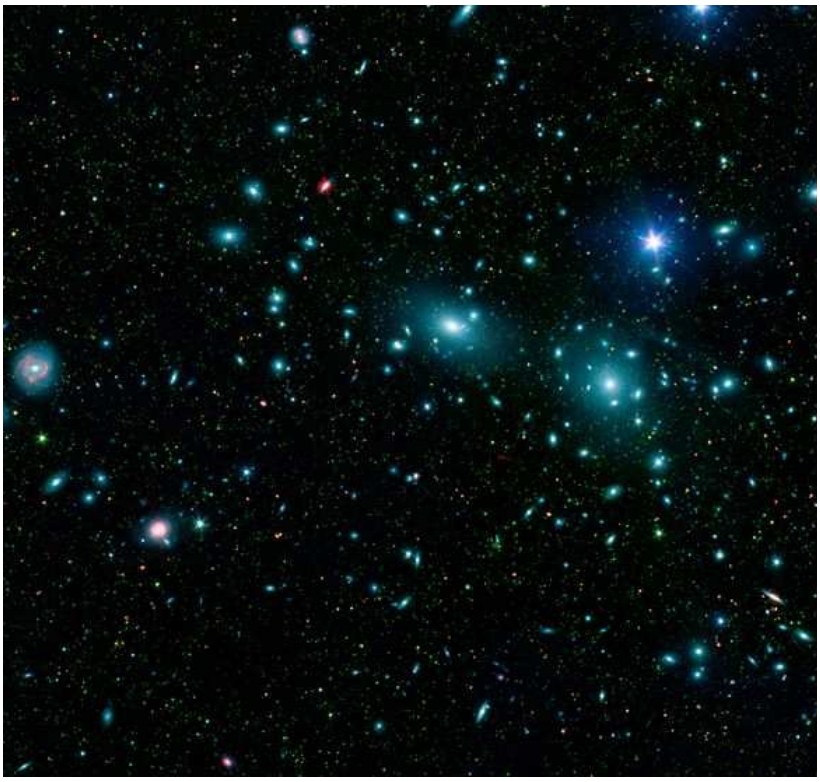

FIG. 1: A photograph of the Coma galaxy cluster.

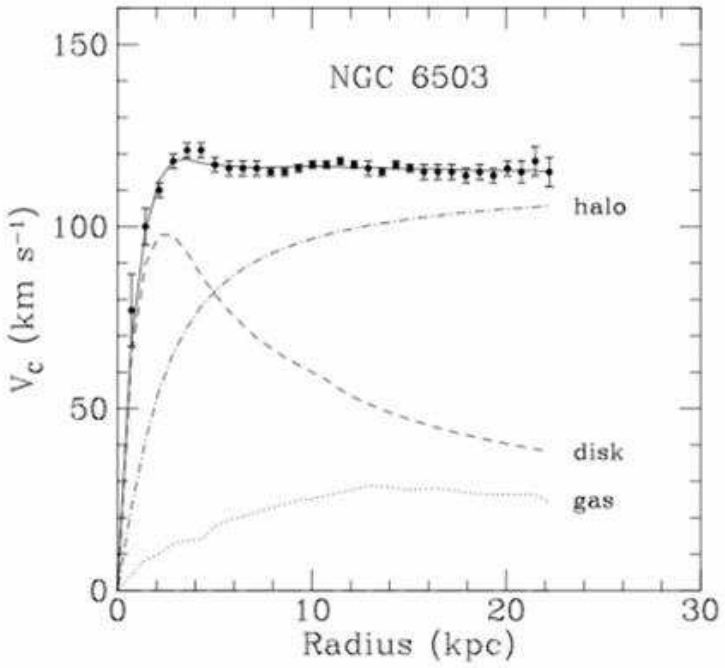

FIG. 2: Rotational curve of spiral galaxy NGC 6503.

II. XENON DARK MATTER SEARCH EXPERIMENT

The XENON Dark Matter Search Experiment is a direct detection experiment of dark matter searching for WIMPs (Weakly Interacting Massive Particles), which are good candidates for dark matter that are hypothesized by super-symmetry (SUSY). WIMPs are examples of massive non-baryonic cold dark matter, or non-relativistic dark matter that does not usually interact with luminous matter and is estimated to be about 100 times the mass of a proton. SUSY predicts that the neutralino is the best WIMP candidate, as it is the lightest super-symmetric particle and stable when R parity is conserved.

The XENON detector is a dual-phase time projection chamber that operates in the following manner: Particles enter the detector and elastically scatter off the target xenon nuclei in the liquid phase, ionizing the xenon and creating the primary scintillation pulse (S1). The ionization electrons then drift upwards towards the secondary gas phase of the detector by an applied electric field, where the secondary proportional scintillation signal (S2) is produced (see Figure 3). Xenon is used, among other reasons, because of its high atomic number, which gives it a high stopping power to reject signals from gamma-rays and other background sources [1].

III. INTRODUCTION TO MY WORK

This report summarizes the work I did for the Columbia University REU at Nevis Labs during the summer of 2007, under the direction of Dr. Elena Aprile as part of the XENON collaboration. I worked on two projects: the first of which was to refine the XENON10 simulation with activated xenon data and the second of which was to test Hamamatsu avalanche photodiodes (APDs).

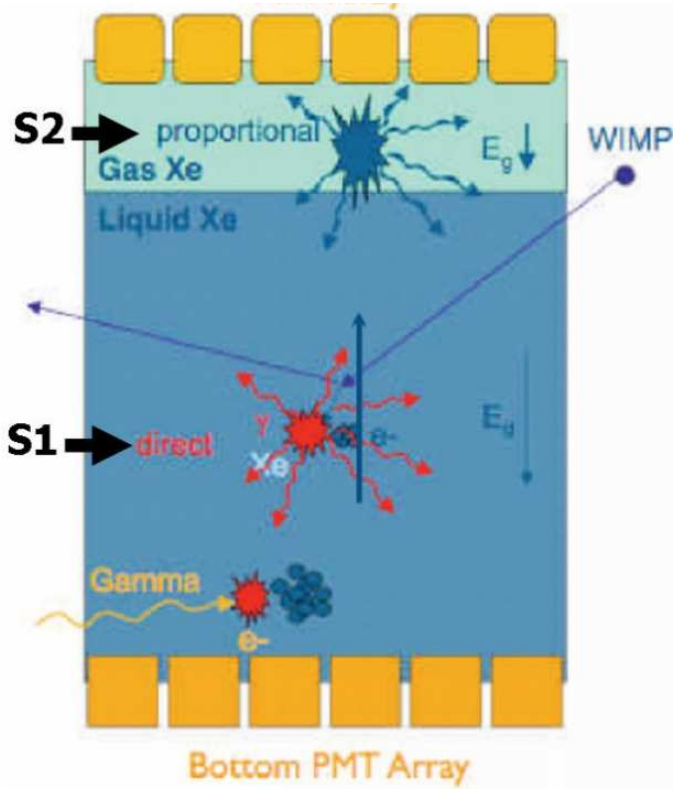

FIG. 3: Illustration of the possible signals from the liquid xenon time projection chamber.

IV. 1ST PROJECT: REFINING SIMULATION WITH ACTIVATED XENON DATA FOR XENON10

A. Abstract

A Geant4 Monte Carlo simulation has been used to characterize the light response of the XENON10 detector. We refined this simulation by varying the parameters that influence light collection efficiency and comparing each variation to activated xenon (AXe) data. The AXe S1 pulse reaching each photomultiplier tube (PMT) in the bottom array was compared to those of 12 different versions of the simulation by finding the χ^2. The version of the simulation that gave the lowest χ^2 value was found.

B. Activated Xenon Calibration

The XENON10 detector was filled with 450g of gaseous xenon (GXe) and then irradiated for 12 days with a ^{252}Cf source, thus producing activated xenon. This volume was then added to liquid xenon (LXe) to finalize the calibration. Activated xenon creates a uniform, isotropic emission of gamma-rays, which can be used to calibrate the detector. ^{1}29Xe creates a 164 keV photon, while ^{1}31Xe creates a 236 keV photon during the scintillation process.

C. Light Collection Efficiency

The light collection efficiency can be found by the equation

$$A_i(x,y,z) = \frac{E}{W_s}\eta_i(x,y,z)Q_iG_iC_i \tag{1}$$

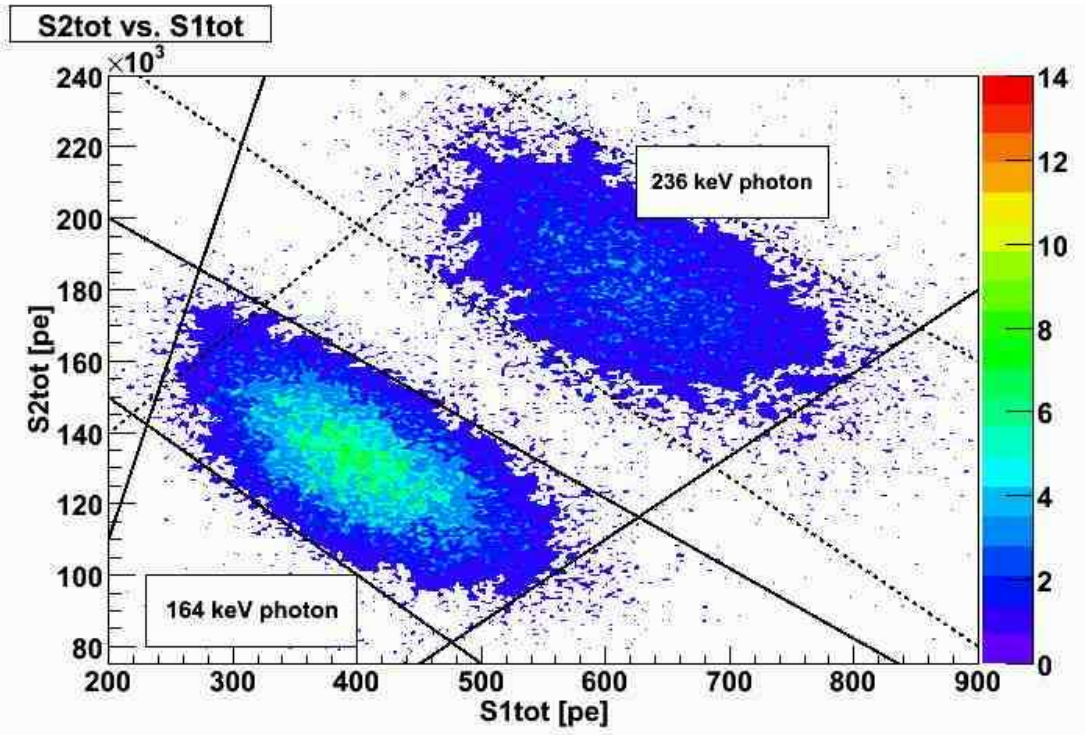

FIG. 4: Total S2 signal versus total S1 signal from AXe data.

where A_i is the amplitude of the PMT signal that reaches PMT i from a given source point (x,y,z), E is the energy deposited, W_s is the energy need to create a scintillation photon, η_i is the fraction of scintillation light that reaches PMT i from a given source point, and Q_i, G_i, and C_i are the quantum efficiency, gain, and collection efficiency of PMT i. Taking the ratio

$$\frac{A_i(x,y,z)}{A_i(0,0,7.5)} = \frac{\eta_i(x,y,z)}{\eta_i(0,0,7.5)} \tag{2}$$

can eliminate the dependence on the other constants, optimizing only the fraction of scintillation light [2]. This ratio was found for the bottom array PMTs in the XENON10 detector for the S1 signal, normalized to the point at the center of the detector.

D. Activated Xenon Data Cut

Only data from the 164 keV photon was used. This cut was obtained by plotting the total S2 against the total S1 and excluding those events not seen in the 164 keV portion of the graph (see Figure 4).

E. Photomultiplier Tube Classes

Taking advantage of the isotropic distribution of events in AXe, the PMTs were grouped into 9 classes (A-I) such that any PMT in a given class could undergo simple reflections or rotations to be in the exact position of the first PMT in that class (see Figure 5). For example, in class A, PMT #63 needs only to be rotated 90 deg in order to be in the same position as PMT #61. Then the S1 signals from all the PMTs in a class from any point in the detector would be similar to each other because each would have the same "view" of the isotropic events in the detector. So the S1 signals from PMTs in the same class could be averaged together, minimizing the number of the computations necessary.

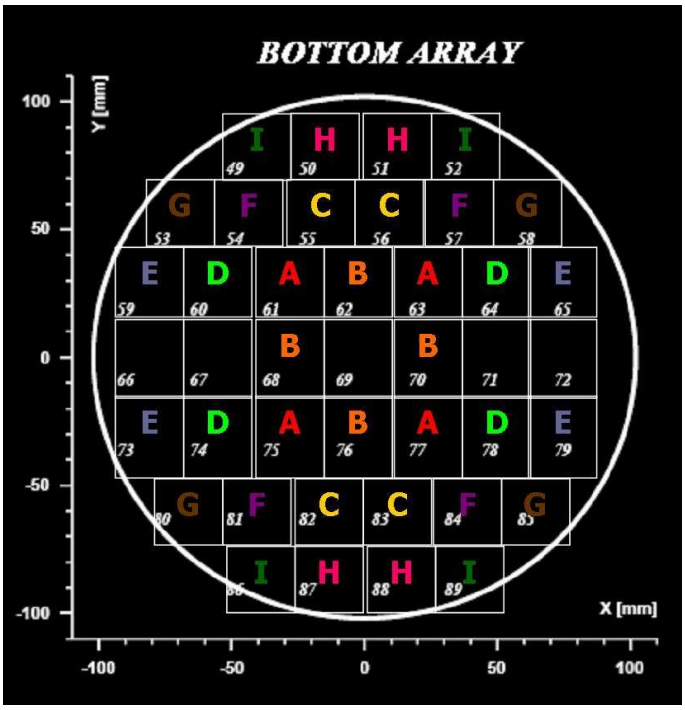

FIG. 5: Bottom array of PMTs and their classes.

F. S1 Signals as a Function of Source Position for Activated Xenon Data and Simulation

The S1 signals relative to the point at the center of the detector were plotted as a function of the source position by making XY-projections of 2D profiles in ROOT (see Figure 6). Through the process of generating these profiles, the detector volume was divided into 847 discrete cells: 11 cells in the x and y directions and 7 in the z direction. Thus, the dimensions of each cell were 1.8 cm x 1.8 cm x 1.9 cm. Each plot in Figure 6 is of a different layer in the z direction. (All initial calculations were done with drift time, as opposed to z distance, and thus 10 μs intervals are labeled on these plots.) Figure 6 displays the S1 signal from the AXe data as a function of the source position for PMT #61, which is a bottom PMT near the center of the detector. This explains why in the 65 to 75 μs range, the highest amplitudes are directly over where PMT #61 is, and why in the subsequent lower drift time ranges, the amplitude progressively gets more spread out.

For better comparison purposes, the profiles were then converted into 1D histograms. Figure 7 displays one such histogram, again for the AXe data from PMT #61. For this plot, each source position was given a number; if one looks again at Figure 6, the first cell in the top left corner of the first profile is source position #1, the cell directly to the right of it is #2, and so on, moving across each row in the x direction in turn. After the 121 positions in the first profile, the next source position comes from the second profile, etc.

Figure 8 compares PMTs #61, 63, 77 and 75, namely the PMTs in class A, once each PMT has been rotated to be in the same position as PMT #61. The amplitudes of the signals from each of these PMTs agree well with each other because, as mentioned above, each has the same perspective of the isotropic events in the detector, and so it was deemed possible to average the signals from each PMT for each class. An example of these averaged histograms is shown in Figure 9. Figure 9 shows the average S1 signal from the AXe data for class A PMTs relative to the center of the detector as a function of the source position.

Figure 9 can be compared to Figure 10, which displays the same plot except for the S1 signal, here renamed PMT hits for distinction purposes, as generated by the simulation. The figures agree well with each other, and so it was possible to find the differences between them by calculating the χ^2.

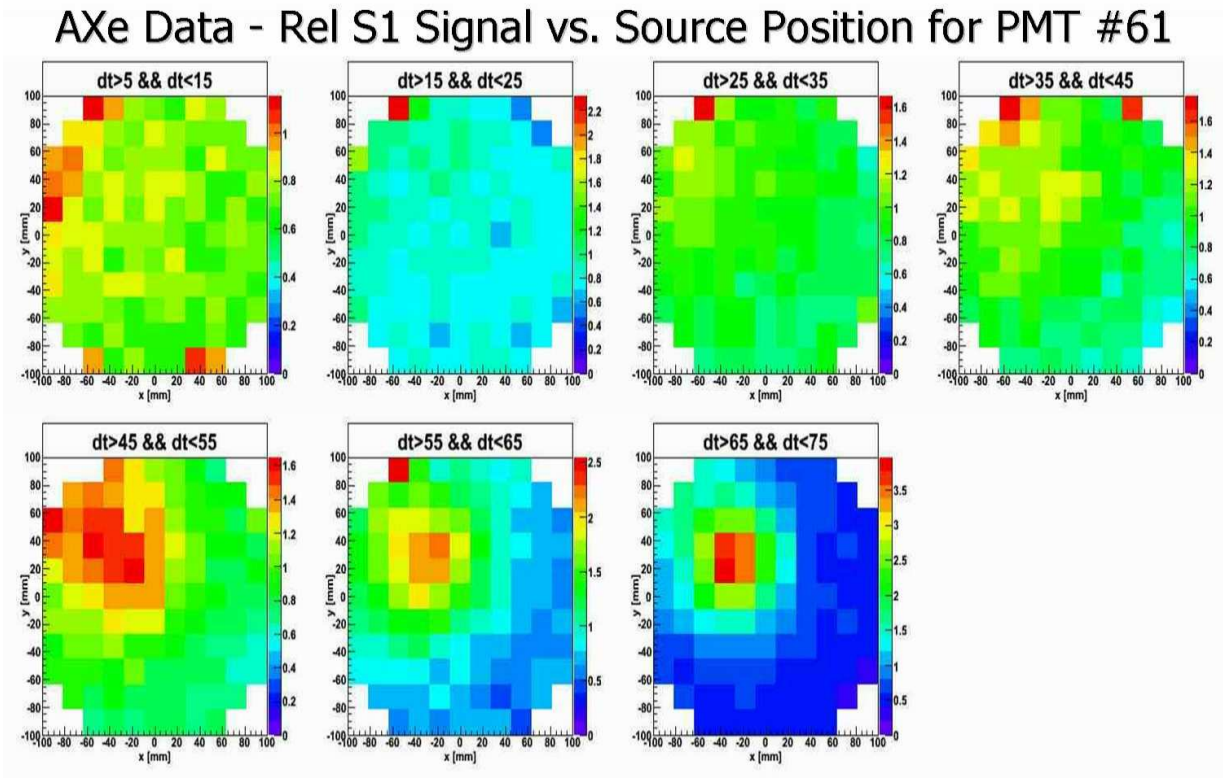

FIG. 6: The S1 signal from the AXe data, relative to the center of the detector, as a function of the source position for PMT #61. Each plot is of a different layer in the z direction.

G. Parameters in Simulation Relating to Light Collection Efficiency

Four different parameters were specified in the different versions of the simulation: Teflon reflectivity and absorption length, Rayleigh scattering, and index of refraction of LXe. The experimental values and the values given the different versions of this simulation of the parameters are displayed in Table I.

TABLE I: The experimental values and the values given the different versions of this simulation of the parameters that influence photon detection.

Parameter	Experimental Value	Values Given in Versions of Simulation
Teflon Relfectivity	0.95 [1]	0.95, 0.975, 1.0
Absorption Length	$>$ 100 cm [3]	50, 100, 125, 150, 200, 300, 500 cm
Rayleigh Scattering	29-50 cm [4–8]	30 cm
Index of Refraction	1.6-1.7 [7–9]	1.69

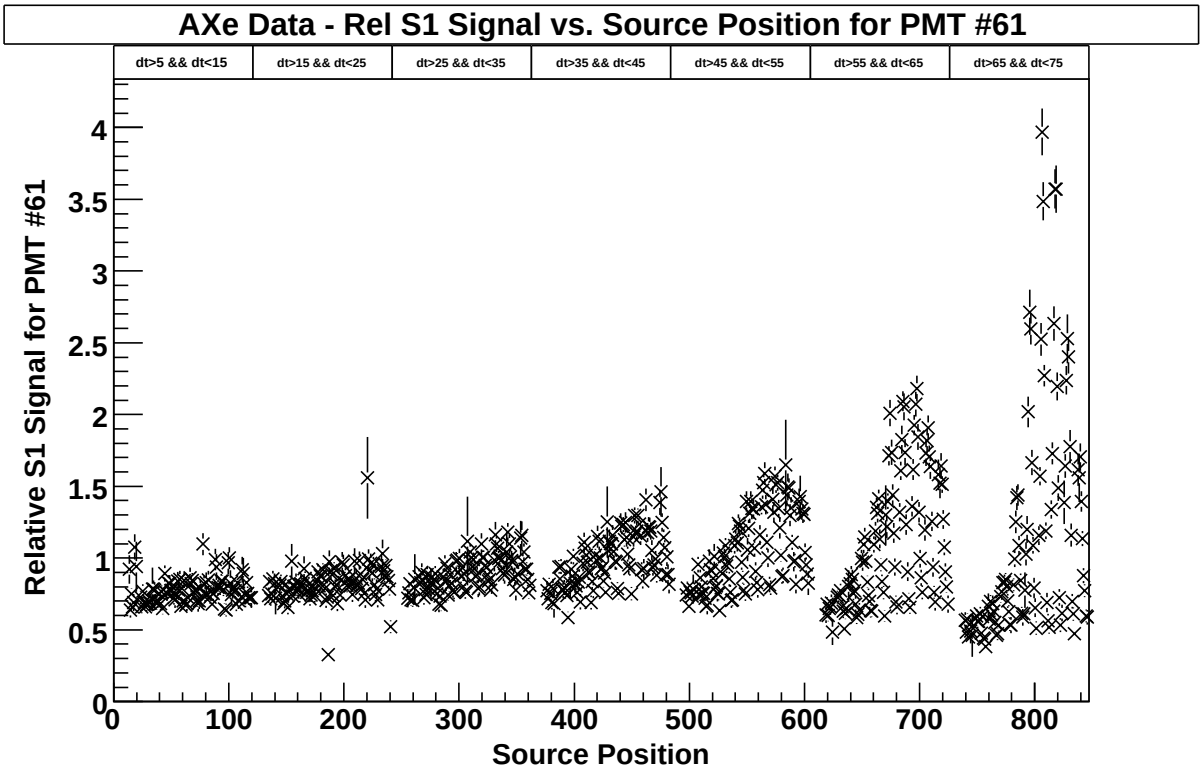

FIG. 7: The S1 signal from the AXe data, relative to the center of the detector, as a function of the source position for PMT #61.

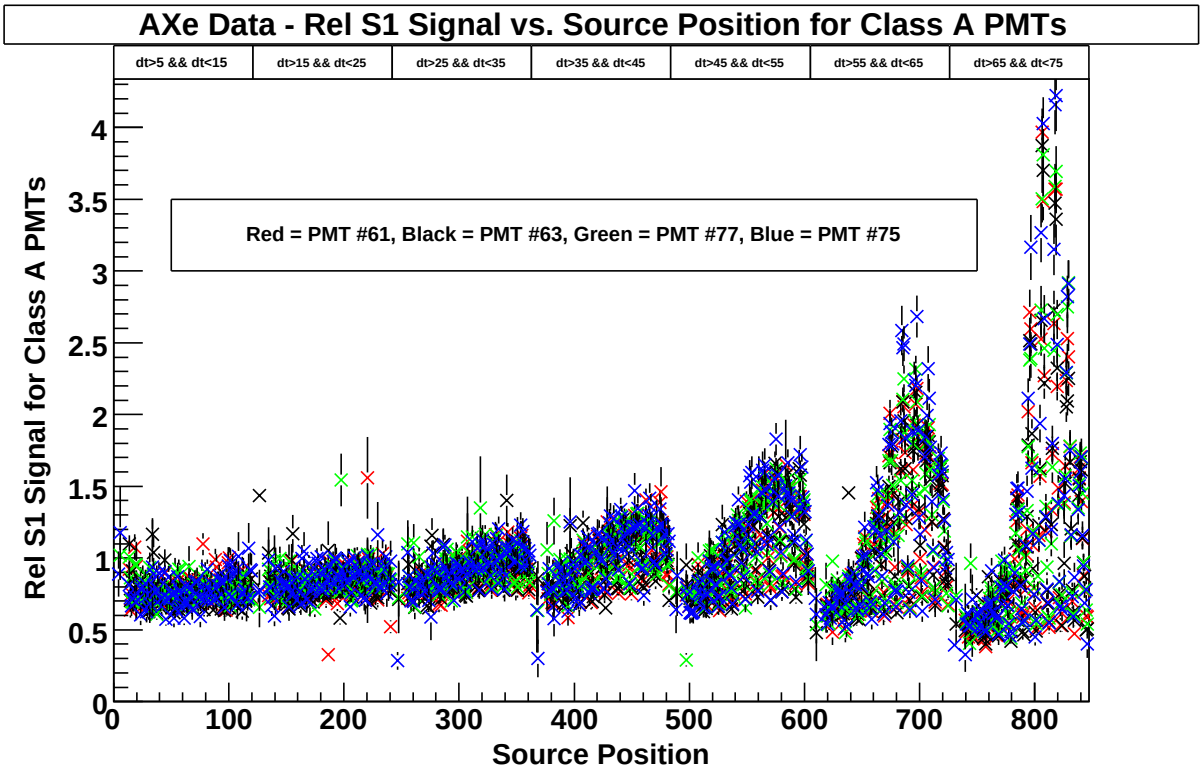

FIG. 8: Comparision of the S1 signal from the AXe data, relative to the center of the detector, as a function of the source position for class A PMTs.

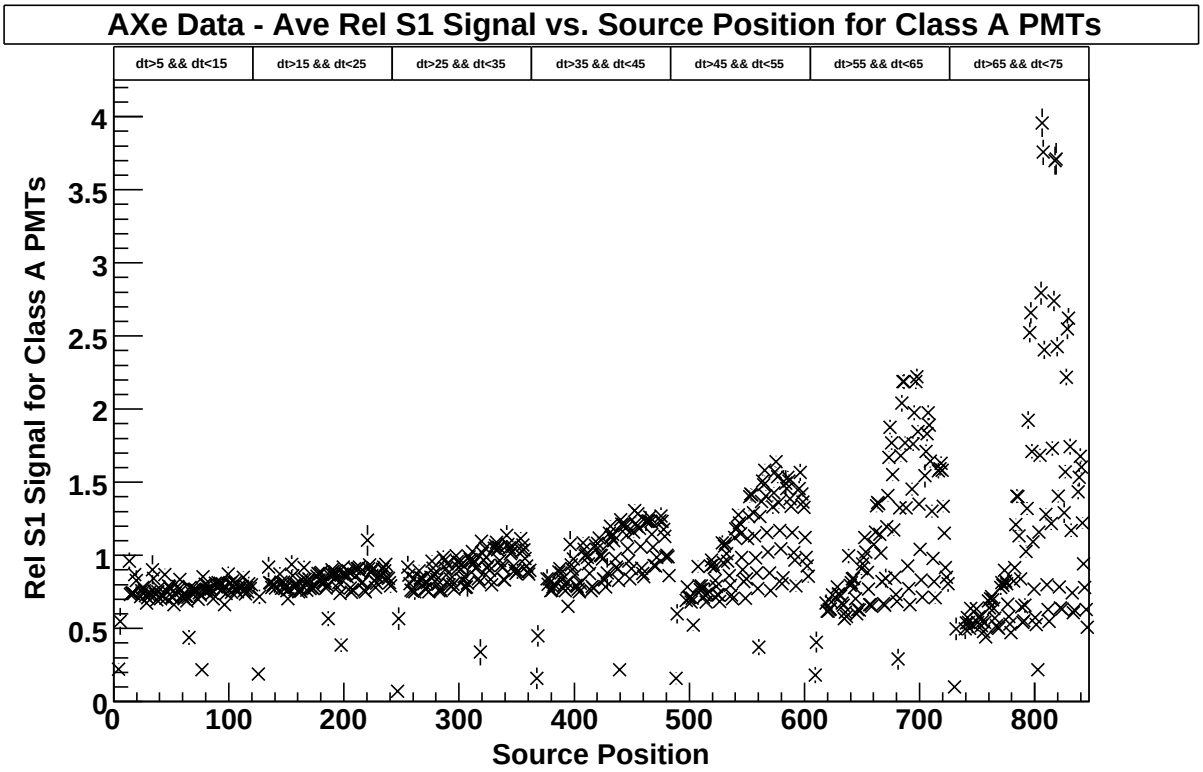

FIG. 9: The S1 signal from the AXe data, relative to the center of the detector and averaged for all class A PMTs, as a function of the source position.

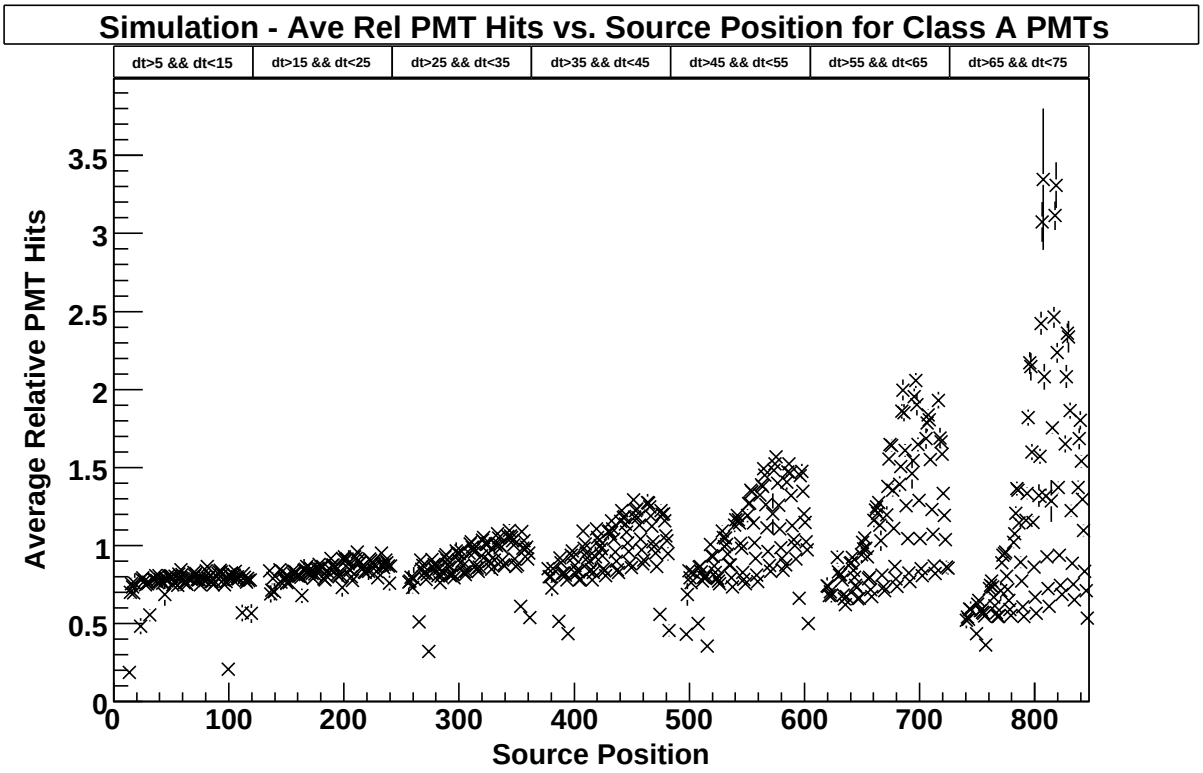

FIG. 10: The S1 signal from the simulation, relative to the center of the detector and averaged for all class A PMTs, as a function of the source position.

H. Results

The χ^2 between the AXe data and the simulation histograms was calculated for each class of PMTs, and then the total χ^2 was found by adding each class's value together. This was done for 12 different versions of the simulation, each version varying the values of some parameters relating to light collection efficiency. These results are listed in Table II. The version of the simulation that is most consistent with the AXe data, out of the ones tested, is simulation #7, which has the parameters 0.95 Teflon reflectivity, 50 cm absorption length, 30 cm Rayleigh scattering, and 1.69 index of refraction.

I. Conclusion

Refining the simulation allows us to better understand what happens in the XENON10 detector and to give us a basis to improve future versions of the detector. The version of the simulation that is most consistent with the AXe data, out of the ones tested, is simulation #7, which has the parameters 0.95 Teflon reflectivity, 50 cm absorption length, 30 cm Rayleigh scattering, and 1.69 index of refraction. Since the absorption length of this version is out of the range specified by the experimental values and since its χ^2 only differs from the χ^2 of simulation #1 by 1.26%, more versions of the simulation should be generated to confirm this result. Future versions of the simulation should continue to vary the parameters specified here, as well as any additional parameters that could influence photon detection. The error in the present analysis could be improved by reducing the volume of each spatial cell, i.e. to values smaller than 6.28 cm^3. This analysis should also be performed again including the top array of PMTs, the S2 signal, and a 236 keV photon cut.

V. 2ND PROJECT: TESTS OF AVALANCHE PHOTODIODES

A. Abstract

We began tests of prototype Hamamatsu APDs in liquid and gaseous xenon, with the ultimate goal of being able to characterize their gain as a function of bias voltage and their quantum efficiency. Most of this work dealt with very preliminary tests, and repeated problems due to noise considerations prevented a complete study of the APDs' properties. Direct alpha particles were detected by the APDs in LXe.

TABLE II: Total χ^2 for each version of the simulation.

Simulation #	**Teflon Reflectivity**	**Absorption Length**	**Rayleigh Scattering**	**Index of Refraction**	**Total χ^2**
1	0.95	100	30	1.69	166191
2	0.95	125	30	1.69	179452
3	0.95	150	30	1.69	196519
4	0.95	200	30	1.69	171445
5	0.95	300	30	1.69	210122
6	0.95	500	30	1.69	178909
7	0.95	50	30	1.69	164090
8	0.975	100	30	1.69	178439
9	0.975	125	30	1.69	178149
10	1.0	100	30	1.69	170085
11	1.0	125	30	1.69	176646
12	1.0	150	30	1.69	176799

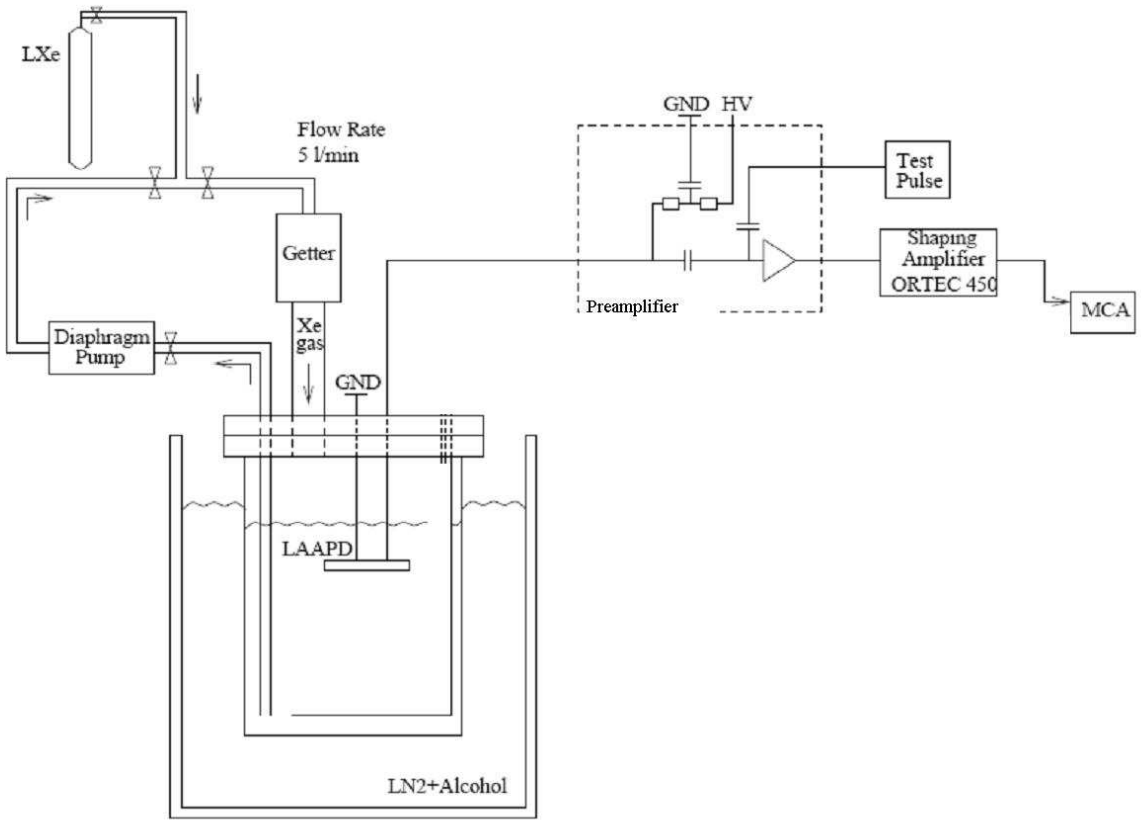

FIG. 11: Schematic drawing of the detector and electronics for the APD tests.

B. Introduction to Avalanche Photodiodes

An avalanche photodiode (APDs) is photodiode that internally amplifies the photocurrent by an avalanche process. APDs may be effective alternatives to PMTs in LXe detectors because of their greater sensitivity, high quantum efficiency and negligible radioactivity contamination. These APDs were tested so that we might determine how effective these APDs would be in LXe and GXe detectors, such as the XENON Dark Matter Search Experiment.

C. Experimental Setup

A schematic drawing of the detector and electronics is shown in Figure 11. The Hamamatsu APDs were placed inside a chamber filled with gas or liquid xenon, and an ^{241}Am α source was placed above the APDs. For the liquid xenon, the chamber was immersed in a liquid nitrogen and alcohol mixture to condense the gas. The APD converted the scintillation light into many photoelectrons, which were then sent to the preamplifier, where they were converted to a charge signal. The charge signals were fed into a low-noise shaping amplifier (ORTEC 450), which amplified the signal, and then to a multi-channel analyzer (MCA) for spectroscopy analysis.

D. Measurements

The linearity of the preamplifier - amplifier - MCA system was verified by measuring the voltage out of the amplifier (final voltage) as a function of the voltage into the preamplifier (input voltage), the MCA channel as a function of the

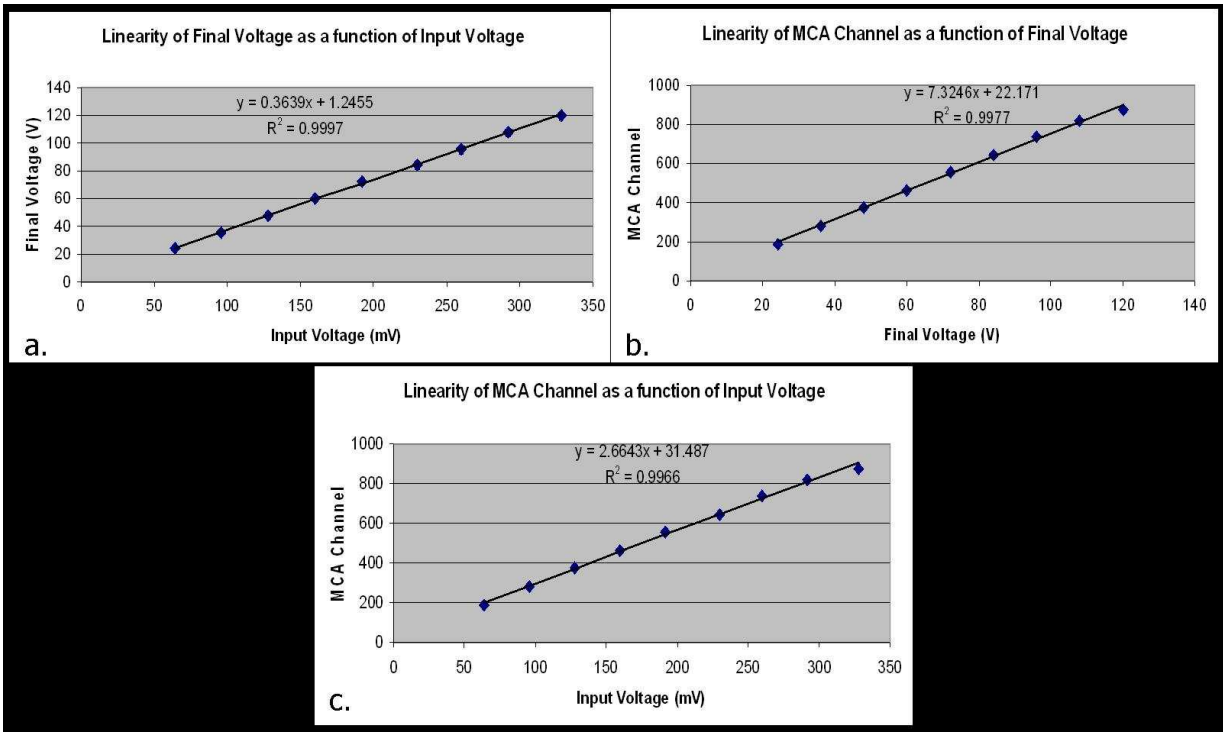

FIG. 12: a. The voltage out of the amplifier (final voltage) as a function of the voltage into the preamplifier (input voltage). b. The MCA channel as a function of the final voltage. c. The MCA channel as a function of the input voltage.

final voltage, and the MCA channel as a function of the input voltage (see Figure 12). Then, the direct scintillation from the alpha source was measured as a function of bias voltage on the APDs when immersed in LXe. A sample spectrum is shown in Figure 13. However, substantial noise interference made it impossible to accurately characterize the APDs' unitary gain.

E. Conclusion

The linearity of the electronic system was verified, and direct alpha peaks, as measured by the APDs, can be discerned in LXe. The data that was taken is inconclusive about the unitary gain measurement due to noise, and so more work is still needed. Some steps that could be taken to reduce the amount of noise are changing preamplifiers and increasing the solid angle between the source and the APD in order to move the charge signal away from the noise peak. Once the noise is minimized, the gain as a function of bias voltage and the quantum efficiency of the APDs could be found.

VI. ACKNOWLEDGMENTS

I would like to thank Professor Aprile and the entire XENON group for all their guidance and help, and for making my summer experience interesting and fun. I would also like to thank John Parsons for organizing the REU program

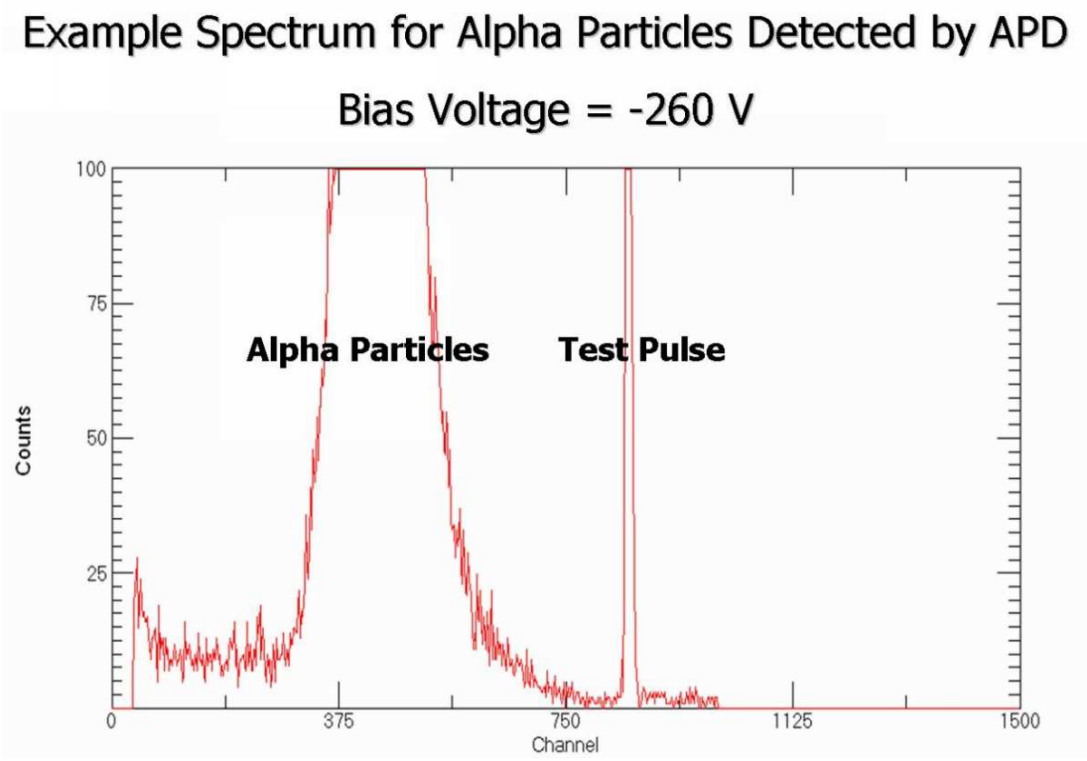

FIG. 13: A sample spectrum showing the direct α-peak and test pulse for a bias of -260 V.

at Columbia and NSF for their grant.

---

[1] *Development of a Liquid Xenon Time Projection Chamber for the XENON Dark Matter Search*, Columbia University, 2006.
[2] Neves, F., *et al.*, *IEEE Trans*, **NS-52**, 2005, 2793.
[3] Baldini, A., *et al.*, *Nucl. Instrum. Methods*, **A545**, 2005, 753.
[4] Braem, A., *et al.*, *Nucl. Instrum. Methods*, **A320**, 1992, 228.
[5] Chepel, V. Y., *et al.*, *Nucl. Instrum. Methods*, **A349**, 1994, 500.
[6] Ishida, N., *et al.*, *Nucl. Instrum. Methods*, **A348**, 1997, 380.
[7] Seidel, G. M., R. E. Lanou, W. Yao, *Nucl. Instrum. Methods*, **A489**, 2002, 189.
[8] Solovov, V. N., V. Chepel, M. I. Lopes, A. Hitachi, *Nucl. Instrum. Methods*, **A516**, 2004, 462.
[9] Barkov, L. M., *et al.*, *Nucl. Instrum. Methods*, **A379**, 1996, 482.